Asian Journal of Physics
Vol. 30, No 1 (2021) 427-444
Available on: www.asianjournalofphysics.in

ap

Recent progress in tissue enhanced spectroscopy for cancer detection

Valery V Tuchin[1,2,3] and Luís M Oliveira[4,5]

[1]*Research-Educational Institute of Optics and Biophotonics, Saratov State University, Saratov, Russian Federation.*

[2]*Interdisciplinary Laboratory of Biophotonics, National Research Tomsk State University, Tomsk, Russian Federation.*

[3]*Laboratory of Laser Diagnostics of Technical and Living Systems,*
Institute of Precision Mechanics and Control of the Russian Academy of Sciences, Saratov, Russian Federation.

[4]*Department of Physics, Polytechnic Institute of Porto – School of Engineering, Porto, Portugal.*

[5]*Centre of Innovation in Engineering and Industrial Technology,*
Polytechnic of Porto – School of Engineering, Porto, Portugal.

Dedicated to Professor Prof V B Kartha,FNA

Spectroscopy methods can be used for pathology identification and monitoring, but their applications are limited by light scattering if the disease is located in deeper tissue layers. The first study presented in this paper shows that the simple application of spectroscopy measurements allows colorectal cancer discrimination through the identification of different pigment content in normal and diseased tissues. The other two studies demonstrate that by combining sensitive spectroscopy measurements in a wide spectral range with optical clearing (OC) treatments is also useful for cancer discrimination. In the second study, by using spectral collimated transmittance (T_c) measurements during OC treatments, it was possible to estimate the diffusion coefficient of glucose in normal and pathological colorectal mucosa as: $D_{glucose}$=5.8×10^{-7} cm^2/s and $D_{glucose}$=4.4×10^{-7} cm^2/s, respectively. An additional result of this study shows that the mobile water content is about 5% higher in pathological mucosa. In the third study, by analyzing the OC efficiency in the deep UV range, it was possible to obtain different protein dissociation rates in normal (27.4) and pathological (79.1) mucosa tissues at 93%-glycerol treatment. Such methods can be applied to study other types of cancer or other diseases, and their conversion into noninvasive procedures, based on diffuse reflectance spectroscopy, is to be expected.

Keywords: Enhanced Tissue Spectroscopy, Colorectal Cancer, Tissue Optical Clearing, Optical Clearing Mechanisms, Optical Clearing Agents.

1 Introduction

Within the diseases that can develop in the human body, cancer-related pathologies are the ones that bring major concern in clinical practice. Due to the high diversity of known cancers, different oncologic specialties have been created throughout the history of medicine. During the development of any cancer, space- and time-dependent changes occur in tissues and cells, leading ultimately to the appearance of malignant tumors [1]. The abnormal cell growth is one of those changes that may lead to the invasion of the surrounding tissues or to the occurrence of metastasis (spread to distant organs), which is the main cause of morbidity and mortality for most patients [1-8]. A considerable number of cancers are known nowadays and their classification regarding the anatomical area where they occur or the associated fatality degree have been reported [9-12]. Since cancer can arise in different anatomical areas of the body without any apparent reason

Corresponding author
e mail: lmo@isep.ipp.pt (Luís M Oliveira)

and spread to other organs, its explanation, detection and control are difficult. Without a clear and precise explanation on how the cancer arises, the establishment of effective prevention and long-term management of these pathologies also becomes difficult [1,10].

Current methods for *in-vivo* cancer detection are mainly based on imaging techniques with ionizing radiation such as positron emission tomography (PET) or X-ray imaging. Alternative *ex- vivo* methods that need tissue excision to perform histopathology analysis are also applied. Considering the great disadvantages that are associated to these methods, the desire for *in- vivo*, noninvasive, non-ionizing and efficient diagnostic methods is high [13].

The use of optical methods for cancer diagnosis has grown significantly during the past 30 years. Figure 1 shows the increasing number of publications that result from searching the expression "*optical cancer detection*" in Google Scholar, Pubmed and Web of Science.

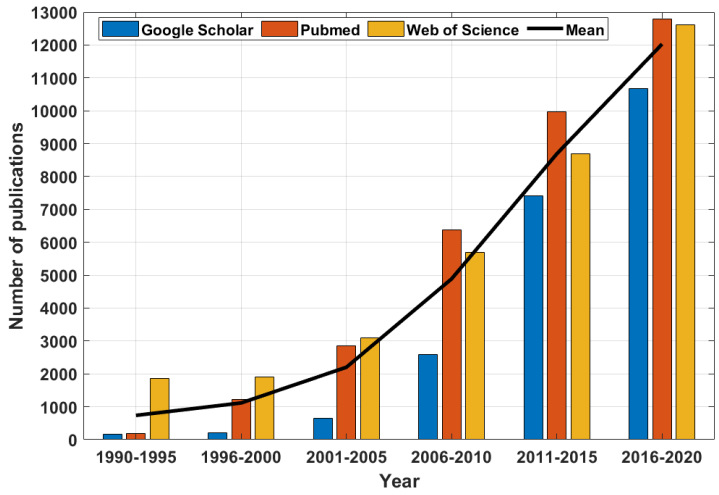

Fig 1. Number of publications in the last 30 years containing the expression "*optical cancer detection*", according to Pubmed, Web of Science and Science Direct.

When the cancer polyps or tumors develop in the outermost tissue layers, noninvasive spectroscopy or imaging methods can be used directly or through endoscopy to perform a diagnosis. Due to the high light scattering that occurs in biological tissues, such procedure will not be effective for cancer detection if the tumors are located deep in the tissue [14]. In the particular case of spectroscopic methods, the spectral signatures that might allow for the establishment of an accurate cancer diagnosis can be difficult to identify. Biological tissues have many absorbers and most of the times, particularly in the ultraviolet (UV), their absorption bands overlap one another [15]. The presence of strong and multiple scattering in biological tissues can also camouflage the discrimination of such useful spectral signatures, obstructing the establishment of a precise diagnosis [16]. As indicted above for precancerous polyps in tissue's superficial layers, the strong light scattering is not a problem in the application of spectroscopy methods, as recently demonstrated by our group with the identification of discriminated lipofuscin-type pigment content in normal and pathological tissues of the human colorectal mucosa [17].

To facilitate the spectroscopy diagnosis of deep-layer cancer tumors, the optical clearing (OC) method can be applied. Such method has been intensively studied for the last 20 years and provided good results in many biological applications, both on *ex vivo* and *in vivo* tissues [14,18]. The application of the OC treatments to tissues, combined with imaging or spectroscopic methods provides new approaches for cancer detection and may allow for early stage diagnosis and cancer progress monitoring [14,19].

The main purpose of the OC treatments is to eliminate light scattering in biological tissues and increase their transparency, allowing to reach deeper light probing depths [14]. Such increase in tissue transparency is obtained through the partial or total replacement of tissue water by a harmless agent, designated as optical clearing agent (OCA), which has a higher refractive index (RI) than water, better matched to the RI of the other tissue components, which are commonly designated as tissue scatterers [14,20,21]. Biological tissues have heterogenous composition, where the various biological components such as lipid droplets, phospholipid membranes, protein fibers and globules, cells and their organelles, like mitochondria and nucleus, are surrounded by the tissue fluids, e.g., the interstitial fluid (ISF) or cell cytoplasm [22]. These fluids are mainly composed of water, in which a small amount of salts, minerals and organic compounds are dissolved [18,23]. Such high water content in tissue fluids, which can reach values above 95% [21], reduces the RI of fluids drastically. Some water is also bound to tissue scatterers to keep their hydration. Such bound water is relatively small, and consequently the RI of tissue scatterers is significantly higher than the RI of tissue fluids. As an example, the RI values of skin melanin and dry proteins in skeletal muscle at 589.6 nm are 1.47 and 1.584 [14,18,24], respectively, while the RI of the ISF in most tissues is of the order of 1.35-1.37 [18]. Such RI mismatch between the ISF and tissue scatterers is responsible for the strong and multiple light scattering in tissues [14].

Several OCAs have proven to be efficient so far in the creation of temporary and reversible transparency in various soft or hard tissues and in blood [14,18]. In terms of safety, and with the exception of some cases reported for some tissues under treatment with highly concentrated solutions of glycerol, dimethyl sulfoxide (DMSO) and propylene glycol (PG) [14,25,26], the great majority of these agents have not induced any side effects in tissues [14,18]. Such OCAs are of various nature, but they can be classified in three main groups: sugars, alcohols and electrolyte solutions [14]. Examples of sugars are glucose, fructose or maltose. Glycerol, sorbitol and PG are OCAs that belong to the group of alcohols, while in the electrolyte solutions, we can find Trazograph^{TM}, Hypaque^{TM} or Verographin^{TM} [14,27]. These and other OCAs, or aqueous solutions that contain them have been tested in various animal and human tissues and the created transparency varies both in magnitude and duration from tissue to tissue. The temporary transparency created by these agents in biological tissues is obtained by the cooperation of the three main mechanisms of OC: tissue dehydration, RI matching and protein dissociation [14].

To understand in detail how the OC treatments reduce light scattering in tissues and to explain the OC mechanisms, we will consider a simple *ex vivo* tissue sample, which was prepared to have a slab-form with a diameter of ~1 cm and a uniform thickness of 0.5 mm. Such sample is used to measure its collimated transmittance (T_c), both in its native state and during treatment to evaluate its kinetics. According to the Bouguer-Beer-Lambert law, T_c is defined as a function of the attenuation coefficient, μ_t, and sample thickness, d [16]:

$$T_c(\lambda) \approx e^{-\mu_t(\lambda)\times d}, \quad (1)$$

where λ is the wavelength and μ_t represents the sum of the absorption coefficient (μ_a) with the scattering coefficient (μ_s).

Considering as a reference the native T_c spectrum for a selected wavelength range, when the tissue sample is immersed in a solution that contains an OCA such as glycerol, we will see an increase in T_c as a result of the OC mechanisms. In the first few minutes of treatment, T_c increases in a fast manner as a result of the dehydration mechanism. Such mechanism is associated to the water loss by the tissue sample, which is induced by the osmotic pressure of the OCA molecules in the treating solution. According to literature [14,28,29], biological tissues are known to contain four stages of water, depending on their bounding strength : strongly bound, tightly bound, weakly bound and free water. The combination of weakly and free water is commonly designated as mobile water, since such water can move to the outside when stimulated by the

osmotic pressure of an OCA during OC treatments [14]. The strongly bound and the tightly bound water, which maintain the other biological component's hydration and provide nutrients to the cells, can also be converted into mobile water to flow out, but to do so, the osmotic pressure of the outside OCA must be maintained for several hours, or days. The fast loss of mobile water at the beginning of the immersion treatment induces a decrease in tissue thickness, which leads to the approximation of the tissue scatterers [14,19,30]. A better organized and more compact packing of tissue scatterers is created inside the tissue sample [16,18,31,32]. Such internal changes can also be obtained by mechanical compression or stretching, since mechanical forces also remove water from the compressed or stretched area of the tissue [14,18]. With the creation of a denser scatterer distribution inside the tissue, an increase in μ_s and μ_a should be expected, but due to a better scatterer ordering inside and to the decreased sample thickness, the transparency of the tissue increases [16,24,30].

As the mobile water begins to move out, it becomes easier for the OCA molecules to initiate their diffusion into the interstitial locations. By having a higher RI than water, the positioning of the OCA molecules in the interstitial locations, close to tissue scatterers, will provide the RI matching mechanism [14,30]. At first, the OCA molecules start to interact with the outermost tissue layers, but with the continuous flux of the water molecules out, the OCA molecules reach deeper inside and will eventually fill all the interstitial areas of the tissue. Studies have demonstrated that the OCA diffusion into the tissues takes several minutes [31,33,34], but during the first few minutes of the treatment, both fluxes (water going out and OCA going in) occur simultaneously, meaning that it becomes necessary to discriminate and characterize them. As a result of the replacement of interstitial water by the OCA molecules, an increase of the mean RI in the ISF will occur, turning it closer to the RI of tissue scatterers – this is the RI matching mechanism. This mechanism is provided by the OCA inclusion in the interstitial locations [31,32,35] and since it decreases light scattering inside, it is also responsible for the increase of tissue transparency [36]. Both the tissue dehydration and the RI matching mechanisms are reversible, since the OCA molecules can be washed out by the water that flows from adjacent tissues *in vivo* or by immersing treated *ex vivo* tissue samples in saline [30]. It has been demonstrated that both the tissue dehydration and the RI matching mechanisms allow for the acquisition of better contrast images from deeper tissue layers [37]. Recent spectroscopic studies performed with human *ex vivo* normal and cancer tissues to discriminate and characterize these mechanisms have also demonstrated a 5% higher content of mobile water in diseased tissues [34,38]. Similar studies performed with tissues from control and diabetic mouse have shown similar results with a higher mobile water content in pathological tissues [39].

A third OC mechanism, which also contributes to the increase of tissue transparency is designated as protein dissociation. Evidence of such mechanism was first detected a few years ago by Choi *et al* [40,41] in a study where multiphoton microscopy was used to generate second harmonic generation (SHG) images from *ex vivo* skin samples under treatment with glycerol solutions. As a result of these treatments, it was observed that collagen dissociation occurs in the extracellular skin matrix due to the action of glycerol. A later study by the same group demonstrated the reversibility of this third OC mechanism, since the reassembly of skin matrix collagen has been observed after sample rehydration in saline [40]. Treatments with other OCAs, such as ethylene glycol (EG) or sorbitol have also demonstrated the occurrence of the protein dissociation mechanism and its reversibility after washing out the OCA [35,41]. Such studies show that the clearing potential of an OCA is related to its protein dissociation capability, proving that the protein dissociation is also an OC mechanism [40-42]. More recent studies show that this mechanism also occurs in other tissues such as colorectal muscle [43] or colorectal mucosa [20]. In this later study, Carneiro *et al* demonstrated that the protein dissociation rate can be discriminated in normal and pathological colorectal mucosa [20]. Such observation of different protein dissociation rates in normal and cancer tissues during OC treatments is to be expected since cancer tissues are known to have higher protein contents than normal tissues [44].

During the past 5 years, our groups, located in Porto (Portugal) and in Saratov (Russian Federation) have performed several *ex vivo* studies from normal and diseased tissues that produced useful information to be considered in future noninvasive optical diagnostic methods for cancer or diabetes detection and progress monitoring. Section 2 describes the methodology applied in these studies to obtain the pathology differentiating parameters and three of those studies, concerning colorectal cancer, are presented in section 3.

2 Experimental methodology

All the studies that produced the results presented in section 3 were conducted with *ex vivo* tissues retrieved from surgical resections of the human colorectal mucosa. The following subsections describe the tissue collection and preparation procedure, the thickness and spectroscopy measurement procedure and the calculations made to obtain the results that discriminate colorectal cancer.

2.1 Tissue collection and preparation

The tissues used in this research were collected from the mucosa, the inner layer of the human colorectal wall. Such tissues were retrieved from surgical specimens of patients under treatment at the Portuguese Oncology Institute of Porto, Portugal. The patient population, to which these studies refer to, contained members of both genders, with ages between 40 and 95.

Following the guidelines of the Ethics Committee of the Portuguese Oncology Institute, the patients have signed a written consent to allow for the use of surgical specimens for diagnose and research purposes.

After collecting the surgical specimens, the normal and pathological areas of the mucosa layer (see Fig 2) were separated from the colorectal wall.

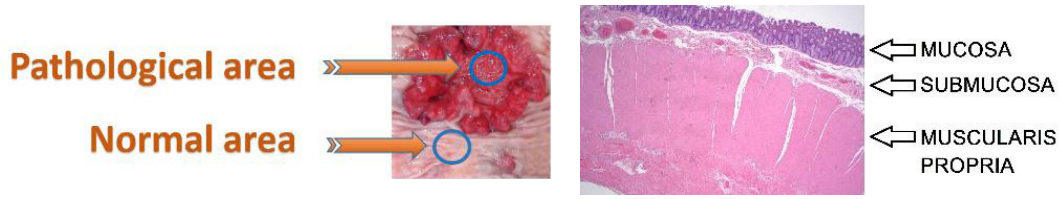

Fig 2. Surgical resection with normal and pathological areas of the colorectal mucosa (left) and microscopy photograph showing the various layers of the colorectal wall (right).

A cryostat was used to prepare the tissue samples from both areas of interest with a slab-form, having an approximated circular shape (ϕ = 1 cm) and uniform thickness of 0.5 mm. Various tissue samples were prepared for each study to allow statistical data.

2.2 Experimental studies

In the various studies, several thickness and spectroscopy measurements needed to be performed. For the first study to estimate the differentiated accumulation of a pigment in normal and pathological mucosa, no OC treatments were applied. In this study, 10 normal and 10 pathological mucosa samples were submitted to total transmittance (T_t), total reflectance (R_t) and T_c spectral measurements [17].

For the second study to obtain the differentiated content of mobile water in normal and pathological mucosa, T_c measurements were made from samples under treatment with aqueous solutions containing glucose in different concentrations: 10%, 15%, 20%, 25%, 30%, 35%, 40%, 45%, 50% and 54%. In each particular treatment with these solutions, measurements were made from 3 normal and 3 pathological mucosa samples to obtain statistical data. To calculate the diffusion coefficients of water and glucose in normal and pathological mucosa, additional thickness measurements were made during treatment with some of the above solutions [34,38].

Since we already knew from previous research [43], that strong OCA osmolarity leads to the creation of a high magnitude UV window between 200 and 260 nm, we planned a new study to evaluate the protein dissociation rate in normal and pathological colorectal mucosa. In this final study, 5 normal and 5 pathological tissue samples were submitted to T_c spectral measurements during treatment with glycerol, 93% pure [20].

The experimental setups and measuring procedures adopted in these three studies are described in the following sub-subsections.

2.2.1 Total transmittance

The measurement of T_t spectra from samples was made with an integrating sphere, as presented in Fig 3.

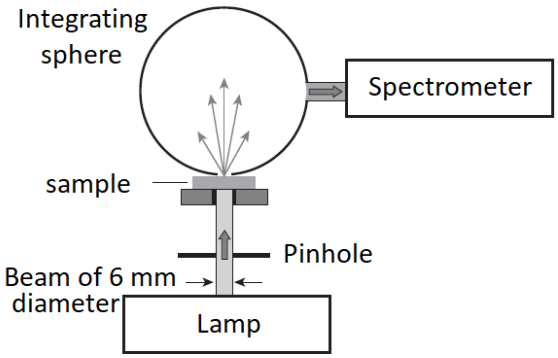

Fig 3. T_t measuring setup with integrating sphere.

A high-power pulsed broad-band xenon lamp was used to irradiate the tissue sample through an optical fiber cable and collimating lens. The pinhole indicated in Fig 3 represents the lens aperture, which limits the beam diameter to 6 mm. The transmitted light that enters the integrating sphere is reflected several times on its inside wall (integration) before being delivered to the spectrometer through an optical fiber cable. All these equipments were purchased from Avantes™ (Netherlands). This setup and measurement procedure were used to obtain the T_t spectra of 10 normal and 10 pathological mucosa samples between 200 and 1000 nm to be used in calculations of the first study presented in section 3.

2.2.2 Total reflectance

To measure the R_t spectra from samples, we used a setup as represented in Fig 4.

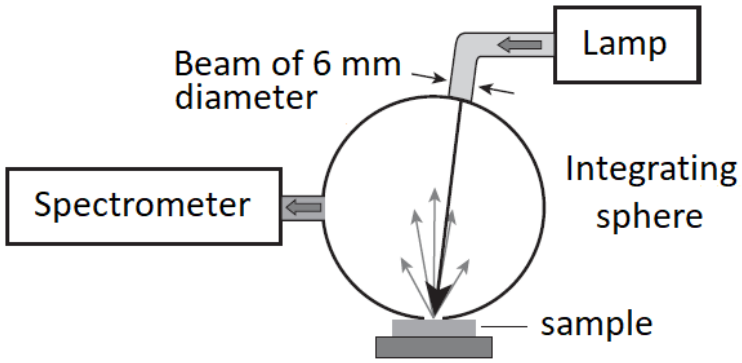

Fig 4. R_t measuring setup with integrating sphere.

Similarly to the T_t measurements, the same high-power pulsed broad-band xenon lamp was used to irradiate the tissue sample through an optical fiber cable and collimating lens. The incident beam reaches the sample at 8º with the vertical axis of the integrating sphere. After the beam is reflected by the sample, it is integrated inside the sphere (multiple reflections in the inside wall), before being delivered to the optical fiber that is connected with the spectrometer. Once again, 10 normal and 10 pathological mucosa samples were submitted to these measurements to acquire their spectra between 200 and 1000 nm. Those spectra were used in the first study presented in section 3.

2.2.3 Collimated transmittance

To acquire the T_c spectra, which were necessary for the second and third studies presented in section 3, we used a setup like the one represented in Fig 5.

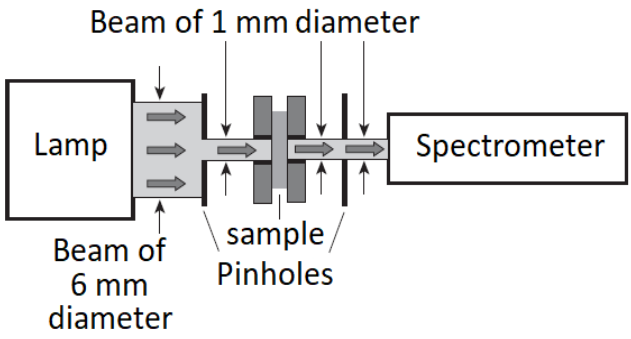

Fig 5. T_c measuring setup.

In these measurements, a beam from a broad-band deuterium halogen lamp (also from Avantes™) was delivered to the left side of the sample through an optical fiber cable and collimating lens. The 6 mm collimated beam that exits the lens passes through a pinhole to reduce its diameter to 1mm, before irradiating the tissue sample. The unscattered beam that is transmitted by the tissue is collected by another optical fiber cable through a second pinhole and another collimating lens. The fiber cable delivers the beam to a spectrometer to register spectra between 200 and 1000 nm. All the space between the two pinholes is inside a dark cuvette that prevents the entrance of ambient light and can be filled with the OC solution to perform measurements during treatment. The four dark-grey rectangles on both sides of the sample in Fig 5 represent a mechanical system to fix the sample at the center of the cuvette. Although this cuvette was built in black plastic to avoid the entrance of ambient light, the entrance and exit of the light beam in the cuvette chamber is made through two special glasses that have flat transmittance (above 90%) through the entire spectral range of interest (200 to 1000 nm). For the measurement of the T_c spectra from native samples, the setup is used as represented in Fig 5. During treatments, the cuvette is filled with the OC solution to immerse the sample before starting the measurements, which are programed to acquire spectra at each 5s during 30 min.

2.2.4 Thickness measurements

In the study to obtain the mobile water content in normal and pathological mucosa, we also have estimated the diffusion times and diffusion coefficients of water and glucose in the normal and pathological mucosa tissues. To calculate the diffusion coefficient (described in section 2.4), thickness kinetic measurements were also necessary for some treatments. To perform those measurements the tissue sample was introduced in-between two microscope glasses as represented in Fig 6. The two glasses had a fixed thickness (d_G = 1 mm), but to prevent excessive force over the sample during measurements, the one on top had a smaller area (1.5 × 1.5 cm^2) than the one at the bottom (1.5 × 7.5 cm^2) [38].

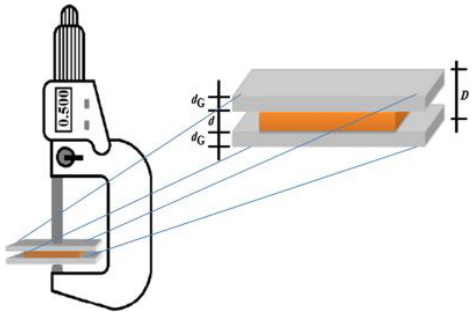

Fig 6. Thickness measuring setup.

The two glasses with the tissue sample in between were placed amid the tips of a precise digital micrometer (precision of 0.001 mm) to evaluate thickness variations. The micrometer was adjusted to have 2.500 mm (2mm from the glasses + 0.500 from the tissue sample). To initiate thickness kinetic measurements, a significant amount of the desired *OC* solution was injected in-between the glasses to immerse the entire sample and initiate the treatment. The micrometer was adjusted smoothly to measure new thickness values at each 15s in the first 2 min and at each min after that. Considering normal mucosa tissues, thickness measurements were made during treatment with 40%- and 54%-glucose. From pathological mucosa tissues, those measurements were acquired during treatment with 35%- and 54%-glucose. Three sets of measurements were acquired in each case to obtain statistical data for the thickness kinetics variation [34,38].

2.4 Calculations

After all experimental data was acquired for each study, some calculations needed to be performed.

Considering the first study to evaluate the differentiated accumulation of a pigment in normal and pathological mucosa, we first used the T_t and R_t spectra obtained from each tissue in Eq (2) to calculate the wavelength dependence for the absorption ($Ab(\lambda)$) [17]:

$$Ab(\lambda) = 1 - \left(\frac{T_t(\lambda) + R_t(\lambda)}{100}\right). \tag{2}$$

Dividing $Ab(\lambda)$ by the sample thickness (0.05cm), we obtained the wavelength dependence for μ_a ($\mu_a(\lambda)$) of each tissue. Comparing the ratios between the hemoglobin peaks at 415 and 550 nm and the minimal value of $\mu_a(\lambda)$ in the near infrared (NIR), we observed that such ratios were significantly low when compared to others previously published for similar mucosal tissues [45]. Such difference between our results and published data means that some pigment has accumulated in the colorectal mucosa tissues used in our study, camouflaging the true blood content. By obtaining information from the patient records at the Portuguese Oncology Institute of Porto, we found that due to a natural product that was administered to the patients in the two days previously to the colorectal surgery, some lipofuscin-type pigment was detected in the complementary histological analysis. By finding the wavelength dependence of μ_a for lipofuscin ($\mu_{a\text{-}pigment}(\lambda)$) in literature as measured for other tissues [46], we reconstructed it as in Eq (3), to subtract it to $\mu_a(\lambda)$ of the normal mucosa and obtain appropriate ratios for the absorption bands of hemoglobin in this tissue.

$$\mu_{a\text{-}pigment}(\lambda) = A \times e^{(3.524 - 0.0187 \times \lambda)}. \tag{3}$$

In Eq (3), $\mu_{a\text{-}pigment}$ is represented in cm^{-1} and λ in nm. A represents the percentage content of the pigment in the tissue, which in the case of normal mucosa assumes the value 1 (100% content). Considering A as 1.1 (110% content) in Eq (3), we were able to subtract $\mu_{a\text{-}pigment}$ to the $\mu_a(\lambda)$ of the pathological mucosa to obtain proper hemoglobin ratios at 415 and 550 nm, resulting in a higher blood content for this tissue as

expected [17]. The results of this study are presented in section 3.

In the second study to calculate the mobile water content in normal and pathological mucosa, we used both thickness and T_c kinetics data obtained from the various treatments with glucose solutions. Considering a wavelength range between 600 and 800 nm, where normal and pathological mucosa present an almost linear increasing T_c with wavelength, we selected individual wavelengths at each 25 nm to calculate the T_c kinetics for each treatment. When calculating these kinetics, we used the mean spectra from three studies for each particular treatment [34,38]. The T_c kinetics data set for each individual wavelength was adjusted with a curve as described by Eq (4) [38]:

$$T_c(\lambda,t) = \frac{C_a(t)}{C_{a0}} \cong \left[1 - \exp\left(-\frac{t}{\tau}\right)\right], \tag{4}$$

$$\text{with } \tau = \frac{d^2}{\pi^2 D_{OCA/water}}, \tag{5}$$

where $C_a(t)$ is the OCA concentration inside the tissue at a particular time of treatment t, C_{a0} is the initial OCA concentration in the treating solution, τ is the characteristic diffusion time of the effective global flux between the treating solution and the tissue, d is the sample thickness at a time of treatment that corresponds to τ and $D_{OCA/water}$ is the characteristic diffusion coefficient of that effective global flux [38]. Since we wanted to discriminate the characteristic diffusion properties (τ and D) for water and glucose in the mucosa tissues and did not know the exact glucose concentration in the treating solution to induce a unique OCA (or water flux) between the treating solution and the tissue, we needed to try various solutions with different glucose concentrations. For each treatment with a particular solution, we obtained various τ values in the fittings of the T_c kinetics data for each selected wavelength with Eq (4). By averaging the various τ values obtained in each treatment and representing the mean τ as a function of glucose concentration in the treating solution for each tissue, we could get a dependence that provided a maximum and a minimum τ value. For a particular tissue, the maximum τ value is the characteristic diffusion time of glucose and the minimum τ value is the characteristic diffusion time of water in that tissue. Such τ values that were retrieved from those graphical representations were then used in Eq (5) to calculate the diffusion coefficients of glucose and water in the normal and pathological mucosa tissues. In these calculations we considered the corresponding thickness values (d) obtained at a time of treatment equal to τ and for the treatment with the same glucose concentration as the one that provides the minimum (for water) and the maximum (for glucose) τ values for each tissue [38]. The results of this study are presented in section 3 and they show that the maximum τ for treatments applied to the normal and pathological mucosa tissues occur at different glucose concentrations in the treating solution. Such difference between normal and pathological mucosa implies different mobile water content in the two tissues, as explained in section 3, and can be used as a discriminating parameter for cancer detection.

In the third study, we also measured T_c spectra from normal and colorectal mucosa tissues, but now during treatments with glycerol (93% pure) [20]. Since proteins have a strong absorption band between 200 and 230 nm [13,46], it was necessary to evaluate the kinetic variations in such deep-UV range. We have observed that the T_c variations in this spectral range were not perceptible when compared to the variations observed in the visible-NIR range. To overcome this problem, we needed to calculate the relative variations of tissue spectra over the time of treatment. We have called such relative variations as optical clearing efficiency (OC_{eff}), and its calculation for the entire spectral range was made using Eq (6) [20,43]:

$$OC_{eff}(\lambda,t) = \frac{T_c(\lambda,t) - T_c(\lambda,t=0)}{T_c(\lambda,t=0)}, \tag{6}$$

where $T_c(\lambda,t)$ is the T_c spectrum of the tissue acquired at time of treatment t and $T_c(\lambda,t=0)$ is the T_c spectrum of the native tissue ($t = 0$). From previous studies [43], we learned that such OC_{eff} is much higher in the

deep-UV range when compared to the visible-NIR, which indicates that the scattering reduction in this range is also more efficient. Due to this strong scattering reduction in the deep-UV, we were able to evaluate the protein dissociation mechanism in normal and pathological mucosa tissues. During this evaluation and considering the wavelength of 200 nm, where the OC_{eff} presented the highest values for both tissues, we retrieved a discriminating parameter, which we called the protein dissociation rate. First, we observed that for both tissues under a 30 min treatment, such kinetics can be characterized by a combination of an initial square-root dependence with a later linear dependence on time [20]. We also observed that the kinetics data at this wavelength for both tissues presents an almost perfect linear fitting between 3 and 10 min. With the objective of developing future noninvasive and fast optical methods for cancer diagnosis, we analyzed the slope of that linear fitting for both tissues. The pathological tissue presented a significantly bigger slope than the normal tissue for that linear fitting, which indicates a higher protein dissociation rate in the pathological tissue as a consequence of the greater protein content as reported in literature [44]. Section 3 presents the results and discussion for this research.

3 Results and discussion

Since we have performed three studies that provide discriminating results that can be used for colorectal cancer diagnostics, the results and discussion from each of these studies will be presented in the following sub-sections.

3.1 Pigment as a marker of colorectal cancer

In this first study, 10 normal and 10 pathological mucosa samples were submitted to T_t and R_t measurements with the setups presented in Fig 3 and in Fig 4, respectively. The mean spectra and standard deviation (SD) bars of these measurements are presented in graphs of Fig 7 for both tissues [17].

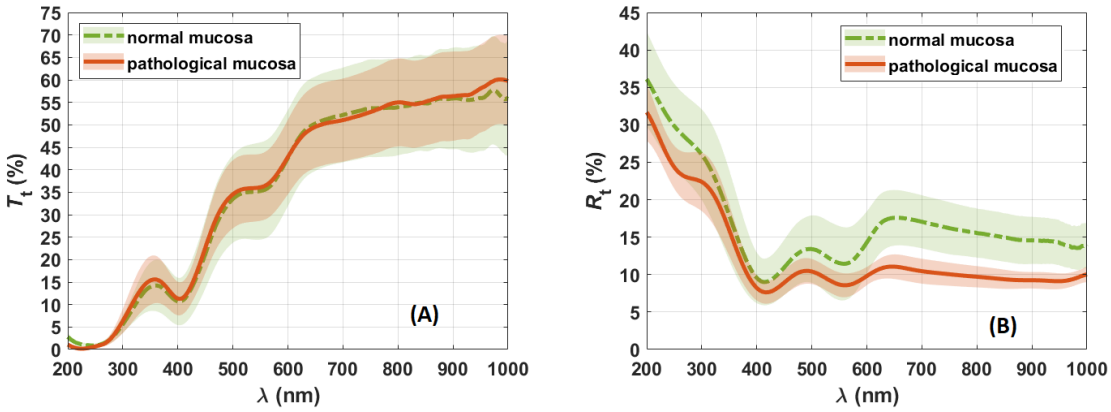

Fig 7. Mean spectra for the normal and pathological mucosa: T_t (*A*) and R_t (*B*).

Using the individual T_t and R_t spectra that originated the mean results presented in Fig 7 in Eq (2) and dividing the result by the sample thickness (0.05 cm), we obtained the wavelength dependency of μ_a for all tissue samples (both normal and pathological). Figure 8 presents the mean $\mu_a(\lambda)$ of both tissues and the corresponding SD bars [17].

Analyzing the ratios between the hemoglobin peaks in the visible and the lowest value of μ_a (at 975-980 nm), we obtained for both tissues a 2.7-fold at 415 nm and a 1.8-fold at 550 nm. Comparing these values with similar data for other mucosal tissues in literature [45], our values were too low (~6 × less). Such fact is evidence that both tissues contain some particular absorber that camouflages the true blood content. Knowing from patient's records that such absorber is a lipofuscin-type absorber, we used the reported wavelength

dependence of lipofuscin [47] to adjust it and subtract to $\mu_a(\lambda)$ of the normal mucosa. In this process of adjustment and subtraction, acceptable ratios were obtained at 415 and 550 nm for the corrected $\mu_a(\lambda)$ of the normal mucosa with $\mu_{a\text{-}pigment}(\lambda)$ as described by Eq (3), when A =1. The obtained ratios for the corrected $\mu_a(\lambda)$ of the normal mucosa were 19.7-fold at 415 nm and 10.1-fold at 550 nm. Using the same procedure for the pathological mucosa, and considering an accumulation of the lipofuscin-type pigment 10% higher (A = 1.1 in Equation 3), we corrected $\mu_a(\lambda)$ and obtained the following ratios: 33.1-fold at 415 nm and 17.3-fold at 550 nm [17]. Comparing between the new ratios of normal and pathological mucosa, we see that the pathological mucosa contains more blood as expected [48]. The results of these corrections to $\mu_a(\lambda)$ of the colorectal mucosa tissues are presented in Fig 9.

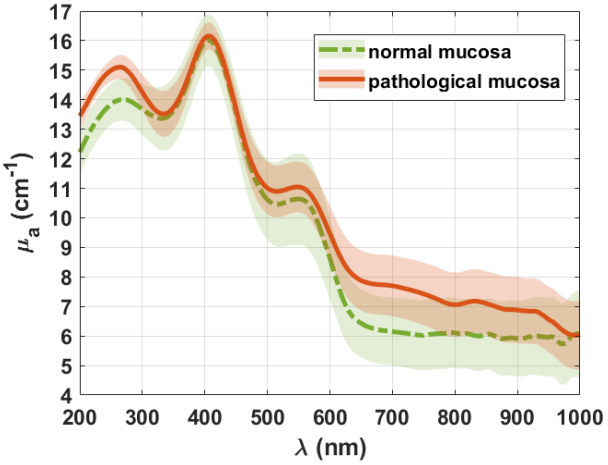

Fig 8. Mean wavelength dependence for μ_a of normal and pathological mucosa.

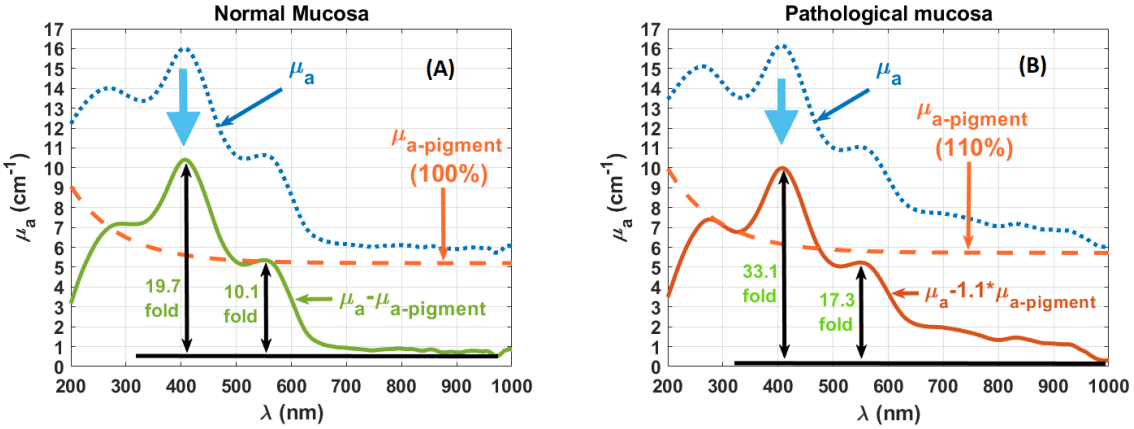

Fig 9. $\mu_a(\lambda)$ for the pigment, for normal (A) and for pathological (B) mucosa, before and after subtracting the absorption of the pigment.

In face of the results produced in this simple study, we can conclude that the detection of discriminated pigment content in colorectal mucosa tissues can be used for the development of noninvasive *in vivo* diagnostic procedures, based on R_d spectroscopy. One of the areas of interest for the future is to estimate $\mu_a(\lambda)$ for tissues from their R_d spectra.

3.2 Differentiated mobile water content in normal and pathological mucosa

In this second study, the colorectal mucosa tissues were treated with aqueous solutions containing different osmolarities of glucose. Three studies were made for each tissue under treatment with a particular glucose osmolarity to obtain mean T_c kinetics at discrete wavelengths between 600 and 800 nm [34,38]. Figure 10 presents the mean T_c kinetics for some of the treatments applied to the normal and pathological mucosa.

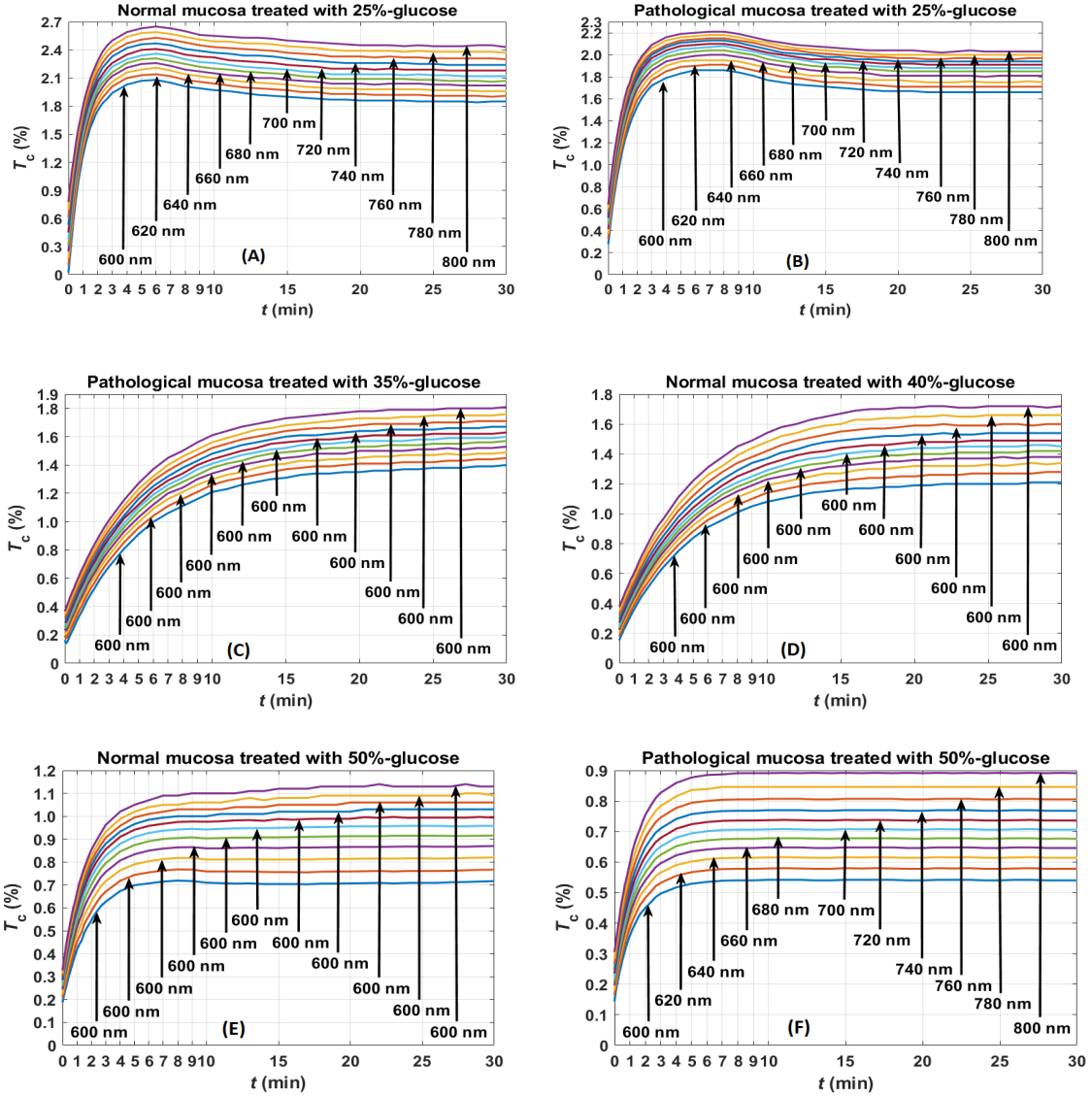

Fig 10. Mean T_c kinetics for the normal and pathological mucosa under treatment with: 25%-glucose (A and B), 35%-glucose (C), 40%-glucose (D) and 50%-glucose (E and F).

As we can see from the various graphs in Fig 10, for treatments with low glucose osmolarity, T_c increases to reach a maximum value after a few minutes of treatment. A smooth decrease is seen after the occurrence of such maximum, indicating a possible water back-flux and tissue swelling into the tissue. Such

time dependence indicates that the effective glucose flux into the tissue is limited in time. From graphs (A) and (B) in Fig 10, we see that such time limit ends at 6 min for the normal mucosa and at 8 min for the pathological mucosa. In alternative, if the treatment is made with intermediate osmolarities, a smooth increase in T_c is observed during the entire treatment. Such behavior is seen in graphs (C) and (D) of Fig 10, which correspond to the treatment of pathological mucosa with 35%-glucose and to the treatment of normal mucosa with 40%-glucose. In these treatments, the time span for the effective glucose diffusion into the tissue is the entire treatment time – 30 min; meaning that a unique glucose flux occurs into the tissue as a result of a water balance between the treating solution and the mobile water in the tissue. For treatments with higher glucose osmolarity, we also see that the significant variations in T_c are limited to the first minutes of treatment. For longer times of treatment T_c stays almost unchanged, indicating that no effective net flux occurs at later treatment.

For a particular treatment and considering the time span where the T_c variations show increasing behavior, each kinetics dataset that corresponds to an individual λ was first displaced to have $T_c(\lambda, t = 0) = 0$ and then normalized to the highest value. After these corrections, each dataset could be fitted with a curve described by Eq (4). During such fittings a τ value was estimated per dataset (one per λ). Averaging the τ values for each particular treatment, we obtained the mean diffusion time that is characteristic for the effective flux that occurs in that treatment. After collecting the mean (and SD) values for τ in each treatment of normal and pathological mucosa, we constructed the graph presented in Fig 11 [34,38].

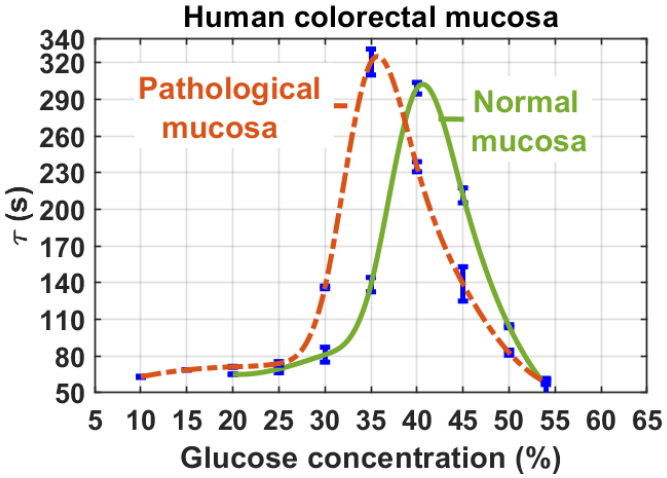

Fig 11. Mean τ as a function of glucose concentration in the treating solution for human normal and pathological colorectal mucosa tissues.

The curves for each tissue in Fig 11 show peaks at different glucose concentrations in the treating solution. The values at these peaks represent the true diffusion time of glucose in the corresponding mucosa tissues. From the graph, we retrieved the characteristic diffusion times of glucose as 325.1s in pathological mucosa and 302.4s in the normal mucosa. The characteristic diffusion time of water was retrieved from each curve at the highest glucose concentration (54%) as: 58.4s in the pathological mucosa and 55.7s in the normal mucosa.

To calculate the corresponding diffusion coefficients of water and glucose in the normal and pathological tissues with Eq (5), we needed to perform thickness kinetic measurements. Since the peaks in Fig 11 occur at glucose concentrations of 35.7% and 40.6% in the treating solution, we performed the thickness measurements for pathological mucosa under treatment with 35%-glucose and for normal mucosa under

treatment with 40%-glucose. Similar thickness measurements were made for both tissues under treatment with 54%-glucose to estimate the diffusion coefficients of water. The mean of three thickness studies (in each treatment) are presented in graphs of Fig 12.

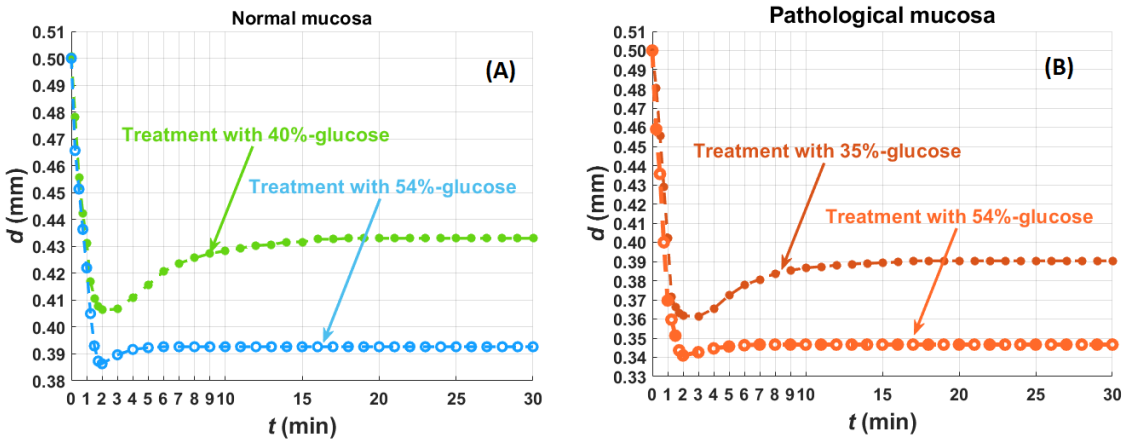

Fig 12. Mean thickness kinetic measurements from mucosa tissues: normal mucosa under treatment with 40%-glucose and 54%-glucose (A), and pathological mucosa under treatment with 35%-glucose and 54%-glucose.

Considering the mean kinetics in graphs of Fig 12 and retrieving the thickness values that correspond to the time of treatment that match the various τ values of glucose and water as estimated from Fig 11, we used Eq (5) to calculate the corresponding diffusion coefficients. The results of these calculations were: $D_{glucose} = 5.8\times10^{-7}$ cm^2/s and $D_{H_2O} = 3.3\times10^{-6}$ cm^2/s in normal mucosa and $D_{glucose} = 4.4 \times 10^{-7}$ cm^2/s and $D_{H_2O} = 2.4\times10^{-6}$ cm^2/s in pathological mucosa [14,34,38]. As we can see these values are different for the two tissues, meaning that such information can also be used to discriminate colorectal cancer.

Finally, and considering the concentrations that correspond to the peaks in Fig 11, we can calculate the mobile water content in both tissues. It is known that the unique OCA flux into the tissue occurs when the water in the treating solution is balanced by the mobile water in the tissue. This way, no water flux occurs into or out-from the tissue. For the normal mucosa, the τ peak occurred at a glucose concentration of 40.6%. This means that the water content in the solution and consequently the mobile water in the mucosa is 59.4%. For the pathological mucosa, the τ peak occurred at a glucose concentration of 35.7%, indicating a mobile water content in this tissue of 64.3% [34,38]. These results show that pathological tissues have higher content of mobile water than normal tissues, and the discrimination of these values can also be used as a diagnostic parameter for colorectal cancer. Similar results for τ can be obtained from the kinetics of noninvasive R_d measurements. The thickness kinetics can also be obtained noninvasively through OCT [14], meaning that such procedure can be adapted to perform noninvasive evaluation of the diffusion properties of OCAs in tissues and estimate the mobile water content.

3.4 Differentiated protein dissociation rate in normal and pathological mucosa

In this final study, 5 normal and 5 pathological mucosa samples were submitted to T_c spectral measurements during treatment with 93%-glycerol [20]. The spectra were acquired between 200 and 1000 nm. Representing these spectra as a function of the time of treatment, the T_c variations in the UV range, where proteins have a strong absorption band (200-230 nm [13,46]) were neglectable when compared to the variations in the visible-NIR range. To access the kinetic variations in this deep-UV range, we used Eq (6) to calculate the OC_{eff} in each tissue. To perform these calculations, we used the mean spectra from each tissue (mean of 5 studies). Figure 13 presents the calculated OC_{eff} for both mucosa tissues.

According to the graphs in Fig 13, the calculated OC_{eff} presents the highest magnitude in the deep-UV as a result of the protein dissociation and RI matching mechanisms. The values observed in these graphs show higher magnitude for the pathological mucosa, a result that makes sense if we remember that cancer tissues have higher protein content than normal tissues [44].

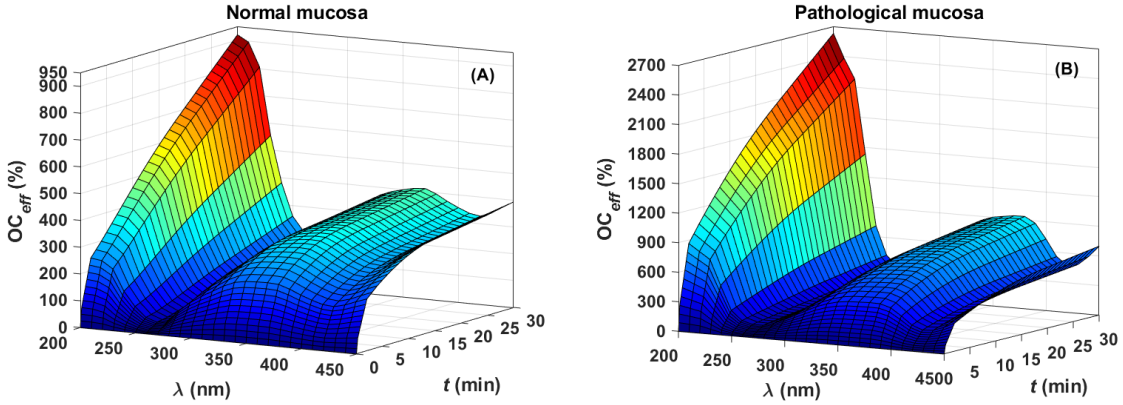

Fig 13. Mean OC_{eff} kinetics for the treatments of normal mucosa (A) and pathological mucosa (B) with 93%-glycerol.

Considering that the protein absorption band occurs at 200-230 nm and that from graphs in Fig 13 we see that the highest OC_{eff} values are located at 200 nm, we selected this wavelength to perform further analysis and try to discriminate the pathology. By representing the OC_{eff} kinetics at 200 nm for both tissues, we saw that such kinetics are well fitted by a curve that has a square-root time dependence at the beginning and a linear time dependence at later times of treatment [20]. Considering that future noninvasive diagnostic procedures, based on this analysis should be fast, we observed that a linear time dependence can be used to fit the OC_{eff} kinetics of both tissues for the time range between 3 and 10 min. Figure 14 presents the OC_{eff} kinetics (blue points and SD bars), the global fitting based on the combination of a square-root and linear dependencies (orange lines) and the linear fitting between 3 and 10 min (light-blue lines) for both tissues [20].

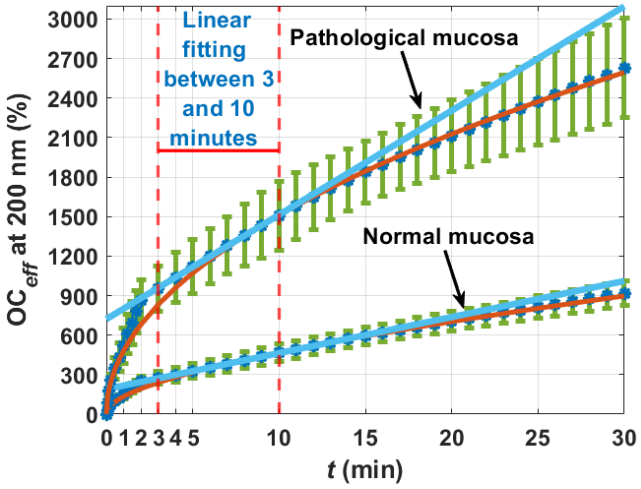

Fig 14. Mean OC_{eff} kinetics at 200 nm for normal and pathological mucosa at 93%-glycerol treatment, dual time dependence fitting for the entire treatment (orange lines) and linear fitting between 3 and 10 min (light blue lines).

The curves for the linear fittings of OC_{eff} kinetics data from both tissues in Fig 14 are described by the following equations [20]:

$$OC_{eff\text{-}nm} = 27.4 \times t + 189.6, \quad (7)$$

$$OC_{eff\text{-}pm} = 79.1 \times t + 721.5, \quad (8)$$

where $OC_{eff\text{-}nm}$ is the OC_{eff} for the normal mucosa, $OC_{eff\text{-}pm}$ is the OC_{eff} for the pathological mucosa, both represented in % and t is the time of treatment, represented in minutes.

Since the slope obtained from these equations is significantly different (27.4 for normal mucosa and 79.1 for pathological mucosa), having the pathological tissue the higher value, we can use it as measure of the protein dissociation rate and a possible parameter for future cancer diagnostic procedures. Since proteins are known to accumulate in a higher proportion in cancer tissues [44], and such accumulation increases with cancer progression, further studies should be made to obtain a calibration curve of the protein dissociation rate as a function of the various stages of cancer development. Such studies should be performed not only for colorectal cancer, but for other cancers as well.

4 Conclusions

The methodology and results presented in the above studies show that colorectal cancer tissues can be discriminated from normal tissues using optical spectroscopy methods. The collimated transmittance T_c was the most useful spectral measurement used in these studies due to its sensitivity to the internal changes that are induced by OC treatments. Although the measurements were performed from *ex vivo* tissue samples, similar procedures can be developed, based on R_d spectral measurements, to develop similar procedures for *in vivo* cancer detection and monitoring.

In the first study, no OC treatments were necessary, since the detection of a pigment that has a characteristic wavelength dependence for absorption can be easily identified with appropriate calculations. In general, such pigments accumulate at the outermost superficial layers of tissues, like skin, oral or colorectal mucosa. For this reason, OC treatments are not necessary to improve the light probing depth in spectroscopy measurements in such studies.

Our initial objective for the second and third studies was to acquire information to characterize the OC mechanisms, but by obtaining discriminating data for normal and pathological tissues, the results have also proven to be valuable for cancer discrimination. Regarding the estimation of water and OCA's diffusion properties in other tissues, we have collected some data from other studies, which is available from the paper on Ref 34, or monograph (see Ref 14), but there are many other tissues and OCAs to study or other pathologies to investigate. Additionally, the conversion of this method to acquire the same diffusion data from noninvasive spectral R_d measurements should be of interest. In the third study, by knowing that cancer diseased tissues accumulate more proteins than normal tissues and that OCAs dissociate proteins, we could obtain discriminating data between normal and pathological mucosa tissues. The application of spectroscopy methods combined with OC treatments to normal and pathological tissues has proven to be a powerful tool for pathology detection and future research will certainly make it useful for the detection of other pathologies, their progress monitoring and control.

References

1. Seyfried T N, Flores R E, Poff A M, D'Agostino D P, Cancer as a metabolic disease: implications for novel therapeutics, *Carcinogenesis*, 35(2014)515-527.
2. Sporn M B, The war on cancer, *The Lancet*, 347(1996)1377-1381.
3. Lichtenstein A V, Strategies of the war in cancer: to kill or to neutralize?, *Front Oncol*, 8(2019)667-1-5; doi. org/10.3389/fonc.2018.00667.
4. Seyfried T N, Cancer As a Metabolic Disease: On the Origin, Management, and Prevention of Cancer, (John Wiley

& Sons, Hoboken, New Jersey, USA), 2012.
5. Fidler I J, The pathogenesis of cancer metastasis: the 'seed and soil' hypothesis revisited, *Nat Rev Cancer*, 3(2003)453-458.
6. Gupta G P, Massagué J, Cancer metastasis: building a framework, *Cell*, 127(2006)679-695.
7. Lazebnik Y, What are the hallmarks of cancer?, *Nat Rev Cancer*, 10(2010)232-233.
8. Tarin D, Cell and tissue interactions in carcinogenesis and metastasis and their clinical significance, *Semin Cancer Biol*, 21(2011)72-82.
9. Parkin D M, Stjernswärd J, Muir C S, Estimates of the worldwide frequency of twelve major cancers, *Bull World Health Organiz*, 62(1984)163-182.
10. Tuchin V V, Popp J, Zakharov V, (Eds), Multimodal Optical Diagnostics of Cancer, (Springer Nature Switzerland), 2020.
11. Ferlay J, Soerjomataram I, Dikshit R, Eser S, Mathers C, Rebelo M, Parkin D M, Forman D, Bray F, Cancer incidence and mortality worldwide: sources, methods and major patterns in GLOBOCAN 2012, *Int J Cancer*, 136(2015)E359-E386.
12. Bray F, Ferlay J, Soerjomataram I, Siegel R, Torre L A, Jemal A, Global cancer statistics 2018: GLOBOCAN estimates of incidence and mortality worldwide for 36 cancers in 185 countries, *CA Cancer J Clin*, 68(2018)394-424.
13. Oliveira L, Tuchin V V, Optical clearing for cancer diagnostics and monitoring, *in Tissue optical clearing: new prospects in optical imaging*, D Zhu, E Genina, V Tuchin, (eds), (CRC Press), 2021.
14. Oliveira L, Tuchin V V, The Optical Clearing Method – A New Tool for Clinical Practice and Biomedical Engineering, (Springer, Cham-Switzerland), 2019.
15. Zhou Y, Yao J, Wang L V, Tutorial on photoacoustic tomography, *J Biomed Opt*, 21(2016)061007; doi.org/10.1117/1.JBO.21.6.061007.
16. Tuchin V V, Tissue Optics – Light Scattering Methods and Instruments for Medical Diagnostics, 3rd edn, (SPIE Press Bellingham, WA, USA), 2015.
17. Carvalho S, Carneiro I, Henrique R, Tuchin V, Oliveira L, Lipofuscin-type pigment as a marker of colorectal cancer, *Electronics*, 9(2020)1805; doi.org/10.3390/electronics9111805.
18. Tuchin V V, Optical Clearing of Tissues and Blood, (SPIE Press, Bellingham, USA), 2006.
19. Genina E A, Oliveira L M, Bashkatov A N, Tuchin V V, Optical Clearing of Biological Tissues: Prospects of Application for Multimodal Malignancy Diagnostics, *in Multimodal Optical Diagnostics of Cancer*, (eds), V V Tuchin, J Popp, V Zakharov, (Springer Nature, Switzerland), 2020.
20. Carneiro I, Carvalho S, Henrique R, Selifonov A, Oliveira L, Tuchin V V, Enhanced ultraviolet spectroscopy by optical clearing for biomedical applications, *IEEE J Sel Top Quant Elect*, 27(2021)7200108; 10.1109/JSTQE.2020.3012350.
21. Gomes N, Tuchin V V, Oliveira L M, Refractive index matching efficiency in colorectal mucosa treated with glycerol, *IEEE J Sel Top Quant Elect*, 27(2021)7200808; doi.10.1109/JSTQE.2021.3050208.
22. Oliveira L, Carvalho M I, Nogueira E, Tuchin V V, Skeletal muscle dispersion (400-1000nm) and kinetics at optical clearing, *J Biophot*, 11(2018)e20170094; doi.org/10.1002/jbio.201700094.
23. Oliveira L, Lage A, Pais Clemente M, Tuchin V V, Rat muscle opacity decrease due to the osmosis of a simple mixture, *J Biomed Opt*, 15(2010)055004; doi.org/10.1117/1.3486539
24. Oliveira L, Lage A, Pais Clemente M, Tuchin V V, Optical characterization and composition of abdominal wall muscle from rat, *Opt Laser Eng*, 47(2009)667-672.
25. Wen X, Mao Z, Han Z, Tuchin V V, Zhu D, *In vivo* skin optical clearing by glycerol solutions: mechanism, *J Biophot* 3(2010)44-52.
26. Zhu D, Larin K V, Luo Q, Tuchin V V, Recent progress in tissue optical clearing, *Las Phot Rev* 7(2013)732-757.
27. Tuchina D K, Meerovich I G, Sindeeva O, Zherdeva V V, Savitsky A P, Bogdanov Jr A A, Tuchin V V, Magnetic resonance contrast agents in optical clearing: prospects for multimodal tissue imaging, *J Biophot*, 13(2020)e201960249; doi.org/10.1002/jbio.201960249.
28. Sdobnov A Y, Darvin M E, Schleusener J, Lademann J, Tuchin V V, Hydrogen bound water profiles in the skin influenced by optical clearing molecular agents – quantitative analysis using confocal Raman microscopy, *J Biophot* 12(2019)e201800283; doi.org/10.1002/jbio.201800283.
29. Choe C-S, Lademann J, Darvin M E, Depth profiles of hydrogen bound water molecule types and their relation to lipid protein interaction in the human stratum corneum *in vivo*, *Analyst*, 141(2016)6329-6337.

30. Yu T, Zhu D, Oliveira L, Genina E, Bashkatov A, Tuchin V V, Tissue optical clearing mechanisms, *in Tissue optical clearing: new prospects in optical imaging*, D Zhu, E Genina, V Tuchin, (Eds), (CRC Press), 2021.
31. Oliveira L M, Carvalho M I, Nogueira E M, Tuchin V V, Diffusion characteristics of ethylene glycol in skeletal muscle, *J Biomed Opt*, 20(2015)051019; doi.org/10.1117/1.JBO.20.5.051019.
32. Oliveira L, Carvalho M I, Nogueira E M, Tuchin V V, Optical clearing mechanisms characterization in muscle, *J Innov Opt Health Sci*, 9(2016)1650035; doi.org/10.1142/S1793545816500358
33. Oliveira L M, Carvalho M I, Nogueira E M, Tuchin V V, The characteristic time of glucose diffusion measured for muscle tissue at optical clearing, *Laser Phys* 23(2013)075606;doi.org/10.1088/1054-660X/23/7/075606.
34. Carneiro I, Carvalho S, Henrique R, Oliveira L, Tuchin V V, A robust *ex vivo* method to evaluate the diffusion properties of agents in biological tissues, *J Biophot* 12(2019)e201800333; doi.org/10.1002/jbio.201800333.
35. Hirshburg J, Choi B, Nelson J S, Yeh A T, Correlation between collagen solubility and skin optical clearing using sugars, *Las Surg Med*, 39(2007)140-144.
36. Genina E A, Bashkatov A N, Tuchin V V, Tissue optical immersion clearing, *Expert Rev Med Devices*, 7(2010)825-842.
37. Cicchi R, Sampson D, Massi D, Pavone F S, Contrast and depth enhancement in two-photon microscopy of human skin *ex vivo* by use of optical clearing agents, *Opt Express*, 13(2005)2337-2344.
38. Carvalho S, Gueiral N, Nogueira E, Henrique R, Oliveira L, Tuchin V V, Glucose Diffusion in colorectal mucosa – a comparative study between normal and cancer tissues, *J Biomed Opt*, 22(2017)091506; doi.org/10.1117/1.JBO.22.9.091506.
39. Tuchina D K, Bashkatov A N, Bucharskaya A B, Genina E A, Tuchin V V, Study of glycerol diffusion in skin and myocardium ex vivo under the conditions of developing alloxan-induced diabetes, *J Biomed Phot Eng*, 3(2017)020302; doi 10.18287/JBPE17.03.020302.
40. Yeh A, Choi B, Nelson J S, Tromberg B J, Reversible dissociation of collagen in tissues, *J Invest Dermatol* 121(2003)1332-1335.
41. Hirshburg J, Choi B, Nelson J S, Yeh A T, Collagen solubility correlates with skin optical clearing, *J Biomed Opt* 11(2006)040501; doi.org/10.1117/1.2220527.
42. Hirshburg J, Ravikumar K M, Hwang W, Yeh A T, Molecular basis for optical clearing of collagenous tissues, *J Biomed Opt*, 15(2010)055002; doi.org/10.1117/1.3484748.
43. Carneiro I, Carvalho S, Henrique R, Oliveira L, Tuchin V V, Moving tissue spectral window to the deep-ultraviolet via optical clearing, *J Biophiot* 12(2019)e201900181; doi.org/10.1002/jbio.201900181.
44. Peña-Llopis S, Brugarolas J, Simultaneous isolation of high-quality DNA, RNA, miRNA and proteins from tissues for genomic applications, *Nat Protocols*, 8(2013)2240-2255.
45. Bashkatov A N, Genina E A, Kochubey V I, Tuchin V V, Chikina E E, Knyazev A B, Mareev O V, Optical properties of mucous membrane in the spectral range 350-2000 nm, *Opt Spect*, 97(2004)1043-1048.
46. Brescia P, "Micro-volume purity assessment of nuclei acids using A260/A280 ratio and spectral scanning protein and nucleic acid quantification", http://www.biotek.com/resources/application-notes/micro-volume-purity-assessment-of-nucleic-acids-using-asub260/sub/asub280/sub-ratio-and-spectral-scanning/, (accessed: November, 2020).
47. Johansson J D, Wårdell K, Intracerebral quantitative chromophore estimation from reflectance spectra captured during deep brain stimulation implantation, *J Biophot*, 6(2013)435-445.
48. Carvalho S, Gueiral N, Nogueira E, Henrique R, Oliveira L, Tuchin V, Comparative study of the optical properties of colon mucosa and colon precancerous polyps between 400 and 1000 nm, in SPIE Proceedings of BIOS-Photonics West 2017: Dynamics and Fluctuations in Biomedical Photonics, Tuchin V V, Larin K V, Leahy M J, Wang R K, (Eds), (SPIE: Bellingham, WA, USA), SPIE PROC vol 10063, p. 10063, 2017.

[*Received*:1.1.2021; *revised recd*:20.2.2021; *accepted*:25.2.2021]